NIH Public Access
Author Manuscript
J Micromech Microeng. Author manuscript; available in PMC 2014 March 01.

Published in final edited form as:
J Micromech Microeng. 2013 March ; 23: . doi:10.1088/0960-1317/23/3/035026.

Microfluidic jet injection for delivering macromolecules into cells

A. Adamo[1], **O. Roushdy**[2], **R. Dokov**[2], **A. Sharei**[1], and **K.F. Jensen**[1]

K.F. Jensen: kfjensen@mit.edu

[1]Department of Chemical Engineering, Massachusetts Institute of Technology, Cambridge, MA, USA

[2]Department of Mechanical Engineering, Massachusetts Institute of Technology, Cambridge, MA, USA

Abstract

We present a microfluidic based injection system designed to achieve intracellular delivery of macromolecules by directing a picoliter-jet of a solution towards individual cells. After discussing the concept, we present design specification and criteria, elucidate performance and discuss results. The method has the potential to be quantitative and high throughput, overcoming limitations of current intracellular delivery protocols.

1. Introduction

Many biological protocols require the insertion into living cells of a variety of macromolecules ranging from nucleic acids to proteins and tracers, but the delivery of macromolecules across the cell membrane remains a challenging task. Current intracellular delivery techniques can be divided into three main categories: biological methods, chemical methods and physical methods[1]. Biological methods rely on the use of an engineered virus to deliver a portion of nucleic acid of interest. They are very effective, but limited to delivering nucleic acids and they need to be, at least in part, re-engineered for each specific application. In addition, they can also deliver unwanted material (e.g. portions of the viral genome) - a significant problem in the context of *in vivo* applications.[2]

Chemical methods rely on an engineered molecule that works as a vector, crossing the cell membrane and carrying inside the cell the compound of interest. These methods are effective in some applications, but they work only for specific compounds (mainly nucleic acids), often rely on endocytosis that can leave much material trapped in endosomes, and are not quantitative, i.e., the specific amount of material delivered to each cell is not known.[3]

Physical methods for delivery include electroporation[4], sonoporation[5] [6], and microinjection[7]. In electroporation cells are exposed for a short amount of time to an electric field that forms pores in the cell membrane allowing diffusion of species into the cytoplasm. The method can be adapted to a wide range of applications and is used extensively. Its main disadvantages are the lack of quantitative delivery, cell toxicity, damage to sensitive delivery materials, and limited success in protein delivery.[8, 9] Sonoporation has been proposed as an alternative to electroporation [5] [6]. This technique works by generating cavitation bubbles that induce membrane poration, but, there have been limited reports of the method's application to date. Microinjection is a process in which the compound of interest is delivered by performing an intracellular injection with a micro-needle. The process is quantitative and it is generally well tolerated by cells. However, it is slow and time consuming, it requires experienced operators (throughput ~100 cell/ hour at most) or costly dedicated equipment, and it is consequently expensive.[10] Its advantages make it the method of choice for very delicate operations such as nuclear transfer in the

NIH-PA Author Manuscript
NIH-PA Author Manuscript
NIH-PA Author Manuscript

NIH-PA Author Manuscript

NIH-PA Author Manuscript

NIH-PA Author Manuscript

context of generation of transgenic animals.[11] Microinjection would likely be the method of choice for intracellular delivery of macromolecules if its main disadvantages of being slow and expensive were eliminated. Efforts to reduce the cost and increase throughput include automated microinjection devices based on robotic systems[12] and microfluidic systems that move cells onto fixed microneedles.[13] Nevertheless, the overall throughput of microinjection based intracellular delivery remains modest and costs remain high.

Here we present a new microfluidic system aimed at eliminating the disadvantages of traditional microinjection (slow and expensive) while retaining its advantages (generally well tolerated by cells and quantitative). The system is designed to achieve intracellular delivery of a solution carrying the macromolecule of interest by directing a picoliter-jet of this solution onto single cells passing through a narrow channel. After discussing the concept and the design specification, we present a prototype and discuss the preliminary results.

2. Device concept

Figure 1 illustrates the device concept. Suspended cells flow into a microfluidic chip and are lined up using a channel with a width comparable to that of the cells of interest. In the top wall of the channel there is a miniaturized nozzle through which a high speed liquid jet can be fired onto cells upon their passage. The jet has a small volume in comparison to the cell volume and contains the compound to be injected. If the jet has sufficient energy to penetrate the cell, it will deliver a portion of its payload inside the cell. The jet is created using a miniaturized nozzle in communication with a chamber where sudden compression of a piezoelectric membrane generates pressure pulses whenever a jet is needed.

3. System design

3.1 Design specifications

Design of the picoliter-jet injector required an estimate of the relevant injection parameters. In the context of biology and medicine, jets have been used as surgical blades[14] or as a means of transdermal drug delivery.[15] Jet penetration depth has been shown to be a function of speed[16] and we therefore assumed jet speed to be the main parameter determining whether a specific cell type was penetrated by the jet. Absence of specific information on cell penetration speeds limited us to order of magnitude estimates of the jet speed along with other relevant parameters (*i.e.,* jet duration and pressures needed to drive the jet). We decided to compensate for the absence of specific information with a design that could accommodate an ample range of operating parameters and thus enable experimental definition of suitable injection conditions.

The order of magnitude of jet speeds that can penetrate a cell membrane can be estimated with a simple model equating the force a jet exerts onto a surface ($\sim\rho V^2 A$, with ρ density of the liquid, V speed of the jet and A cross section area of the jet) with the force needed to rupture the cell membrane. Little information is available on the cell membrane ultimate tensile strength and data reported in literature span over a large range depending on cell types and approaches used for the measurement. Using data from Miyazaki[17], who reports a maximum disruption load of ~1 μN in tensile tests of fibroblasts, and assuming the cell membrane to have a thickness of ~10 nm, we estimated a required penetration speed of 1–5m/s for a jet that is 1–4 microns in diameter.

The diameter of the jet is dictated by the diameter of the nozzle, which is therefore a critical design parameter. A number of factors must be considered in selecting the jet/nozzle diameter. We can expect jets with a smaller diameter to be less toxic to target cells than

NIH-PA Author Manuscript

NIH-PA Author Manuscript

NIH-PA Author Manuscript

larger ones, but such jets will also have a lower flow rate and facilitate the control of the delivered volume. On the other hand, the smaller the nozzle the larger the pressures needed to generate the jet. Moreover, the jet speed depends on the square of the nozzle diameter since the jet is in the laminar flow regime despite its high speed. Additionally, building a feature a few microns wide with a high aspect ratio and in a direction perpendicular to the wafer surface creates significant microfabrication challenges. With these different considerations in mind and the goal of minimizing trauma to injected cells, we decided to create nozzles with a ~2 μm diameter. We first optimized microfabrication on silicon wafers for nozzles of ~4 μm in diameter and then refined the fabrication recipes to obtain diameters of ~2 μm. To generate jets with speeds of a few meters per second through a 2 μm nozzle (with a ~10–35 μm length), the pressure generating system must be able to generate and hold pressures of ~5–40 bar for tens of microsecond.

Once a cell is penetrated, the injection volume can be controlled by varying the duration of the jet and its speed. Microinjection volumes are typically in the order of 1/10 of the cell volume[18, 19], therefore a cell with a diameter of 12 μm should require a 0.1pL injection volume.. Based on our aforementioned design parameters, we calculated that a 10–30μs pulse duration is required to deliver ~0.1pL. These demanding technical requirements shaped the entire design of the system.

3.2 Microfluidic chip

The microfluidic chip along with the pressure generating system represents the core of the "jet-injection" system. The technical specifications required specific choices in terms of materials, fabrication schemes, layout and packaging. In order to withstand the large pressures needed to generate the jet and the fabrication challenges for a nozzle with a diameter of ~2 μm, silicon was selected as the fabrication material of choice for the microfluidic chip. Silicon provides a unique combination of excellent material properties and established fabrication techniques.

The microfluidic chip consists of a straight channel with inlet and outlet for the cells, and a nozzle in the midsection of the channel roof. We built the nozzle orthogonally to the wafer face to facilitate placement in the center of the channel floor. Thus, the nozzle ran from the bottom of the cell channel toward the back side of the wafer (Fig.2 and 3). In order to minimize the fabrication challenge of etching a 2 μm hole through the wafer and to decrease as much as possible the pressure drop across the nozzle itself, we made a hole of larger diameter (100 μm) from the back side and etched the narrow nozzle from the bottom of this larger hole. In this way, we reduced the nozzle length to ~15–35 μm. The chip fabrication (Fig. 2) was carried out on 450 μm thick, 150 mm wafers and it was started with etching of the back side access hole to the nozzle after thick photoresist patterning. Deep reactive ion etching (DRIE) was carried out until the hole had a depth of ~420 μm. Then, nozzles were patterned onto the front side, first onto photoresist and then onto a 1 micron oxide layer (with RIE) that served as a hard mask. The nozzle was then etched until it reached the back side access hole (~ 30 μm of etch). The oxide mask was then stripped with buffered oxide etch (BOE) and the cell channel was etched together with the access holes with conventional DRIE and photoresist masks. Finally, 0.5 μm of thermal oxide was grown onto the wafer before anodic bonding to a Borofloat wafer and dicing of the individual devices.

We went through several chip designs that all followed the general process discussed here. These designs included flow focusing side channels for cell alignment purposes, and channels of different depths and width (Fig 3 B and D). The biological results discussed in this contribution were obtained with a simple channel that had an injection section of 10 μm wide to minimize lateral cell movement. The channel was 15 μm deep and had a nozzle ~2 μm in diameter.

NIH-PA Author Manuscript

NIH-PA Author Manuscript

NIH-PA Author Manuscript

The jet injection chips were completed by compression packaging parts for both cell suspension loading and coupling to the pressure generating unit (fig. 3 A). It is important to consider that, despite its short overall duration, the flow in the nozzle is laminar and most importantly, it can be considered at steady state (the flow reaches steady state in about 1 μs). [20]

3.3 Pressure generating system

The fluid to be injected was contained in an external chamber. This chamber was connected to the microfluidic chip on one side and sealed on the other with a deformable membrane so that a deformation of the membrane upon activation would compress the fluid in the chamber and generate a pressure pulse. In order to produce pL jets of fluid that could penetrate the cell membrane, we needed to generate a pulse of 5–30bars in 10–40μs. We selected a stack of piezoelectric elements (Physik Instrumente) as an actuation mechanism to achieve such pressures and actuation times. The sudden elongation of the piezo forced the membrane to deflect; thus, compressing the volume of fluid and generating the pressure. The volume change required to generate the pressure pulse is proportional to the compressibility of the fluid. We also took into account deformation of the stainless steel pressure chamber itself as the compliant chamber would deform under load, which could significantly reduce the compression of the fluid and the associated volume change.

During operation, a jet of fluid with sub-picoliter volume needed to be ejected during each actuation. The repeated emission of fluid from the loaded pressure generating chamber was not expected to affect the overall pressure performance of the chamber since the compression of the fluid needed to generate the pulse was in the order of several hundreds of nanoliter and the total volume of the chamber was ~100 μL. The ejected volume was therefore negligible compared to the volumes needed for the pressure generation.

The membrane had a central, stiffer part where it contacted the piezo. Finite element simulations were performed to optimize the dimensions of the membrane so that the required deformation could be achieved with maximum stresses below fatigue limits of the material and without buckling. As shown by the finite element analysis in Fig 4 A and B a thin membrane would buckle on the sides and would not be able to adequately compress the fluid present in the chamber.

The chamber was built in stainless steel to decrease the compliance of the chamber itself during loading, and the chamber was equipped with 2 miniature valves for loading of fluid and subsequent chamber sealing (Beswick engineering) (Fig 4 C and D and Fig 5). Pressure pulses were monitored with a pressure sensor (Kulite Semiconductors) that could measure pressure inside the chamber. A strain gauge was attached to the piezo stack to allow monitoring of its deformation. The sudden deformation of the piezo excited vibration of all the elements of the chamber. While a full dynamical analysis of the system was not carried out, natural frequencies of the piezo, of the membrane, and of the pressure sensor were selected outside of the range of operation (>20 kHz).

Sealing of the parts that compose the chamber was achieved with custom made indium o-rings characterized by significantly lower compliance than rubber o-rings. The generation of pressure in the chamber requires the absence of trapped bubbles and degassing of all the fluids inside the chamber. A degassing protocol was implemented for operation of the pressure chamber. In brief, a volume of about ten chamber volumes of degassed ethanol was flown into the chamber followed by an equal amount of degassed, filtered de-ionized water.

From an electrical viewpoint, the piezoelectric actuator behaves as a capacitor. In order to have rapidcharging and discharging of the piezo, we built custom electronics as typical

NIH-PA Author Manuscript

NIH-PA Author Manuscript

NIH-PA Author Manuscript

amplifiers used for piezo actuation could not deliver the instantaneous high power required. The custom parts included fast switches for opening and closing a circuit (custom built by VSHolding LLC, USA) and resistors to adjust the time constant of the RC circuit for achieving the desired charging and discharging times. The power needed for fast actuation was delivered by a large capacitor (>10 times the capacity of the piezo) that worked as a charge storage in parallel with the voltage supply Fig. 6). A typical piezo response time is ~1/3 of the period of its natural oscillation[21]; for our piezo stack this corresponded to ~ 5 microsecond.

4. System Performance

A custom built lab view code allowed us to generate pulses of assigned length to control the high speed switch. We first tested our ability to generate pressure pulses. Fig. 7 shows a typical recording of the signals of the pressure sensor (Kulite Semiconductors) and of the strain gauge (Kulite Semiconductors). The pressure increases quickly and reaches a maximum that can be held essentially constant, if needed. We have verified that different resistances in the charging circuit changed the piezo charging time as theory suggests. The diagram in Fig. 7 shows typical pressure oscillations superimposed to the main pressure variation. These superimposed pressure waves are real and are not an electrical artifact as shown by high speed imaging of picojet production. They are likely to be due to oscillation of parts of the system, including the fluid itself (given that the speed of a pressure wave in water is ~1480 m/s, the travel time of such a wave through the fluid in the chamber from the membrane to the microfluidic chip is ~9 μs). Pressure recordings were carried out at all times to ensure correct chamber behavior.

Extensive testing of the pressure chamber with the aid of the pressure sensor revealed that degassing is critical to achieve expected pressure performance. The presence of bubbles changed the compliance of the chamber drastically reducing the attainable maximum pressure. The indium O-ring proved very successful as their minimal compliance, compared to rubber-based seals, increased the maximum pressure that could be generated. Since differences in the indium seal influenced the frequency of the oscillations in the chamber, we ensured reproducibility by always tightening the chip holder with the same torque. The valves did not appreciably affect the pressure generation except for when a bubble was trapped in them.

In order to visualize the jet, we performed experiments injecting pure water into a sucrose solution. The refractive index differences between the two fluids enabled visualization of the jet in an inverted microscope (Zeiss Axiovert 200) (Fig. 8).

5. Results and discussion

In order to test whether the jet was capable of penetrating a cell, we performed a set of experiments injecting HeLa cells suspended in a potassium free buffer with a solution of a potassium indicator that became fluorescent upon binding with potassium. With the potassium environment, fluorescence would only be expected inside the cells. Hela cells were trypsinized and suspended in a potassium free buffer (150 mM N-methyl-D-glutamide chloride, 10mM HEPES, 10mM Glucose with pH adjusted to 7.4). Cells were aligned in front of the nozzle by visual inspection under the microscope and a solution of the same potassium free buffer and a potassium indicator (100 μM, Invitrogen P1265) was sent through the nozzle. For jets with speed estimated between 5 and 6 m/s, fluorescence appeared instantaneously as the potassium indicator encountered the potassium present inside the cell (Fig. 9). Importantly, slower jets did not penetrate the target cells. The non-

NIH-PA Author Manuscript

NIH-PA Author Manuscript

NIH-PA Author Manuscript

physiological experimental conditions of these initial experiments did not allow investigation of the effect of jet injection on cell viability.

We next attempted to deliver a fluorescently labeled cell impermeable dextran conjugate MW 10000 (D1868, Invitrogen) into Hela cells. Cells were suspended in PBS and the dextran conjugate was dissolved in PBS and sterile filtered before loading into the pressure generating chamber. We transferred treated cells into culture dishes right after injection and assessed viability by assessing the ability of the cells to reattach to the culture surface and retain adherence and fluorescence 24 hours after treatment (Fig. 10).

The results indicate that jet injection can achieve delivery of cell impermeable compounds into living cells without compromising viability. Moreover, they suggest that microfluidic based jet injection could potentially be a new tool for high throughput delivery of cell impermeable compounds into living cells.

In our experiments, we treated only a small number of cells and so cannot estimate the toxicity of the method. An automated cell alignment system that synchronize individual jets with the rapid passing of single cells in front of the nozzle would be necessary to treat larger number of cells and explore toxicity of the method and its variation as a function of the composition of the injected solution. Moreover, more sophisticated biological experiments would be needed to confirm that the injections are tolerated by a variety of cells lines, in particular more difficult to treat cells such as immune cells and primary cells.

6. Conclusions

We have described a prototype of a microfluidic based jet injector designed to deliver macromolecules inside cell by piercing the cell wall with a picoliter-jet. With this first prototype, we have verified the repeatability of the pressure pulses by comparing pressure pulse recordings at the beginning of an experiment and after several hundred bursts. Moreover, we have compared pictures of water fired into sucrose solution after several hundred bursts without finding any identifiable changes. This suggests that the jets are all the same across a large number of cycles. However, the ability of the jet injector to deliver consistently identical amounts of solution into target cells remains to be proven.

Given the characteristic actuation time of the piezoelectric actuator and assuming that an electronic cell alignment system could process signals rapidly enough to inject a jet every 1 ms, it would be reasonable to expect the jet injector to achieve a throughput of 500–1000 treated cells per minute (assuming an injection time of 50 μs).

Acknowledgments

We thank the Deshpande Center for Technological Innovation for financial support as well as NIH grant RC1 EB011187-02 for partial support. Dr. Davide Marini for help in the design of the experiments with the potassium indicator, and Dr. Kishori Deshpande for sharing her silicon microfabrication knowledge.

References

1. Gao X, Kim KS, Liu D. Nonviral gene delivery: what we know and what is next. Aaps J. 2007; 9(1):E92–E104. [PubMed: 17408239]
2. Somia N. Gene transfer by retroviral vectors: an overview. Methods Mol Biol. 2004; 246:463–490. [PubMed: 14970611]
3. Liu D, Chiao EF, Tian H. Chemical methods for DNA delivery: an overview. Methods Mol Biol. 2004; 245:3–24. [PubMed: 14707366]

NIH-PA Author Manuscript

NIH-PA Author Manuscript

NIH-PA Author Manuscript

4. Gehl J. Electroporation: theory and methods, perspectives for drug delivery, gene therapy and research. Acta Physiol Scand. 2003; 177(4):437–447. [PubMed: 12648161]
5. Gac SL, Zwaan E, van den Berg A, Ohl CD. Sonoporation of suspension cells with a single cavitation bubble in a microfluidic confinement. Lab Chip. 2007; 7(12):1666–1672. [PubMed: 18030385]
6. Ohl CD, Arora M, Ikink R, de Jong N, Versluis M, Delius M, Lohse D. Sonoporation from jetting cavitation bubbles. Biophys J. 2006; 91(11):4285–4295. [PubMed: 16950843]
7. Wagner TE, Hoppe PC, Jollick JD, Scholl DR, Hodinka RL, Gault JB. Microinjection of a rabbit beta-globin gene into zygotes and its subsequent expression in adult mice and their offspring. Proc Natl Acad Sci U S A. 1981; 78(10):6376–6380. [PubMed: 6796959]
8. Derfus AM, Chan WCW, Bhatia SN. Intracellular delivery of quantum dots for live cell labeling and organelle tracking. Advanced Materials. 2004; 16(12):961-+.
9. Chou TH, Biswas S, Lu S. Gene delivery using physical methods: an overview. Methods Mol Biol. 2004; 245:147–166. [PubMed: 14707376]
10. King R. Gene delivery to mammalian cells by microinjection. Methods Mol Biol. 2004; 245:167–174. [PubMed: 14707377]
11. Heuwieser W, Yang X, Jiang S, Foote RH. A comparison between in vitro fertilization and microinjection of immobilized spermatozoa from bulls producing spermatozoa with defects. Mol Reprod Dev. 1992; 33(4):489–491. [PubMed: 1472379]
12. http://solutions.us.fujitsu.com/www/news_archive.shtml?aboutus/pressreleases/pr_121305.
13. Adamo A, Jensen KF. Microfluidic based single cell microinjection. Lab Chip. 2008; 8(8):1258–1261. Epub 2008 Jul 1. [PubMed: 18651065]
14. Shekarriz B. Hydro-Jet technology in urologic surgery. Expert Rev Med Devices. 2005; 2(3):287–291. [PubMed: 16288592]
15. Brown MB, Martin GP, Jones SA, Akomeah FK. Dermal and transdermal drug delivery systems: current and future prospects. Drug Deliv. 2006; 13(3):175–187. [PubMed: 16556569]
16. Stachowiak JC, Li TH, Arora A, Mitragotri S, Fletcher DA. Dynamic control of needle-free jet injection. J Control Release. 2009; 135(2):104–112. Epub 2009 Jan 21. [PubMed: 19284969]
17. Miyazaki H, Hasegawa Y, Hayashi K. A newly designed tensile tester for cells and its application to fibroblasts. J Biomech. 2000; 33(1):97–104. [PubMed: 10609522]
18. Brown, KT.; Flaming, DG. Advanced micropipette technilques for cell physiology. Wiley; 1986.
19. Lacal, JC.; Perona, R.; Feramisco, J. Methods and tools in biosciences and medicine. Basel ; Boston: Birkhäuser Verlag; 1999. Microinjection; p. 248
20. Constantinescu, VN. Laminar viscous flow. Springer; 1995.
21. Physik Instrumente General Catalogue. 2005

NIH-PA Author Manuscript
NIH-PA Author Manuscript
NIH-PA Author Manuscript

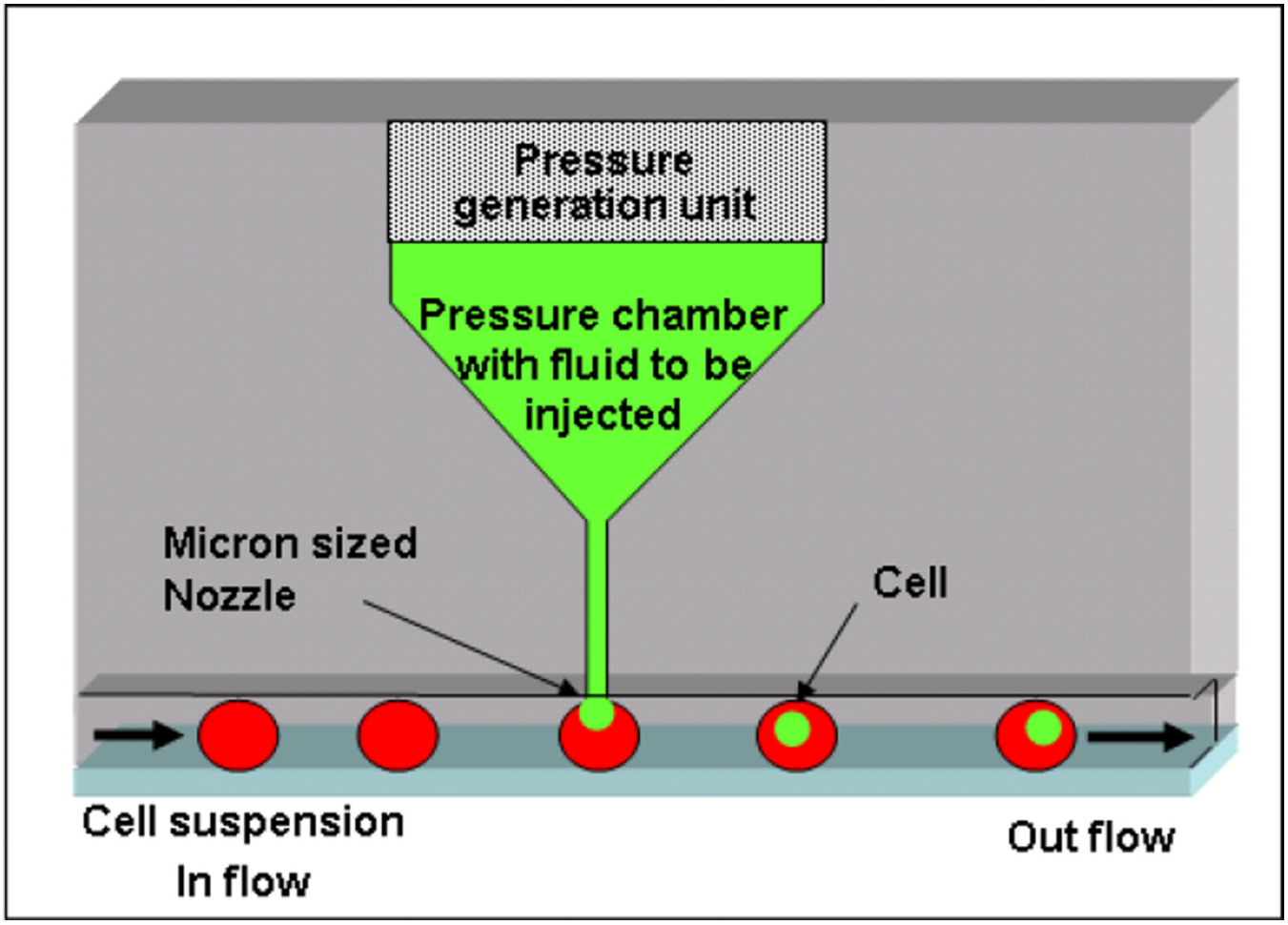

Figure 1.
Schematic illustration of the jet injector. Cells are lined up inside a microfluidic channel with dimensions comparable to the cell size. A miniaturized jet is fired onto the cells to achieve intracellular delivery.

NIH-PA Author Manuscript

NIH-PA Author Manuscript

NIH-PA Author Manuscript

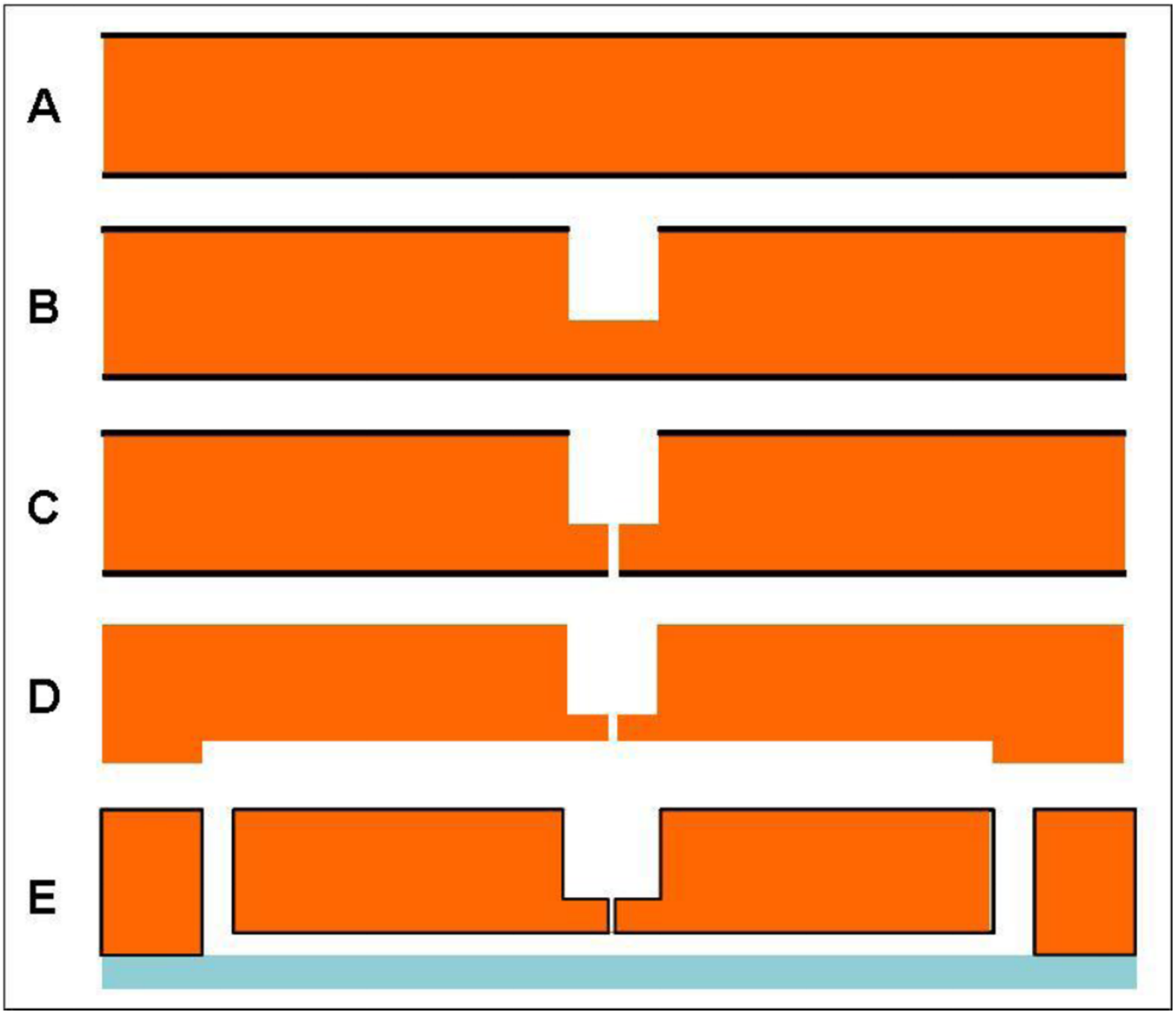

Figure 2.
Microfabrication sequence. A) The process begins with a 450 μm wafer coated with 1 μm silicon oxide (black). B) An access hole to the nozzle is fabricated with deep reactive ion etching (DRIE). C) The nozzle is patterned on the bottoms side first onto photoresist and then onto the silicon oxide that serves as an hard mask for the DRIE nozzle etch. D) Channels for cell flow are patterned onto the nozzle's side E) access holes, thermal oxidation (0.5 μm) and anodic bonding to a Borofloat wafer complete the fabrication.

NIH-PA Author Manuscript
NIH-PA Author Manuscript
NIH-PA Author Manuscript

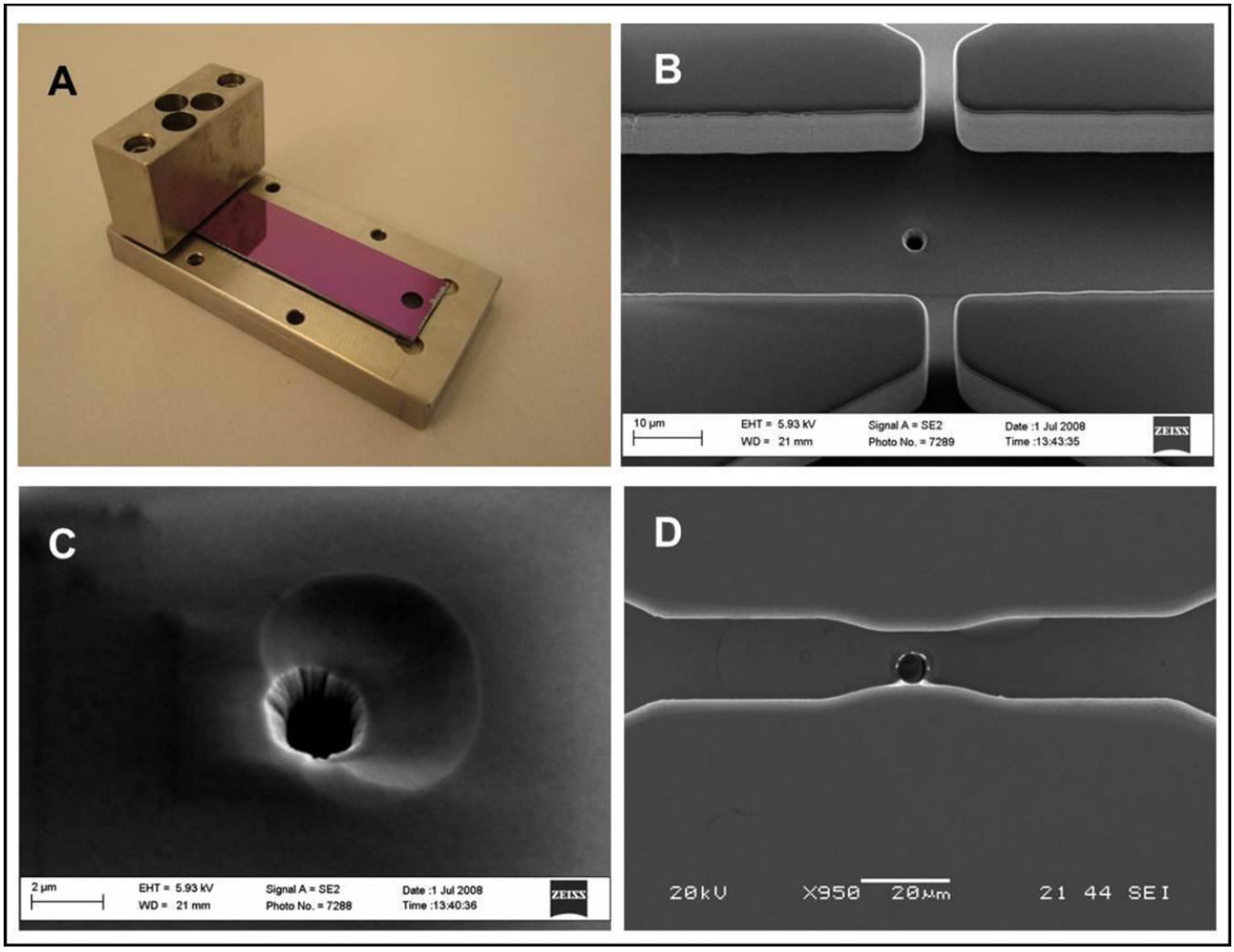

Figure 3.

Microfluidic chip. A) Silicon chip and its holder with inflow supply port. B-C-D) Secondary electron microscopy (SEM) details of the chip in the nozzle area. B) Picture of cell channel. Approximately in the center of the picture the injection nozzle is clearly visible as a dark round spot on the channel wall. The channels coming from the top and the bottom are flow focusing channels (eventually removed from the design). C) Close up of the nozzle. D) Picture of the cell channel. The nozzle is clearly visible slight offset from the center. In this chip the cell channel narrows at the level of the nozzle.

NIH-PA Author Manuscript

NIH-PA Author Manuscript

NIH-PA Author Manuscript

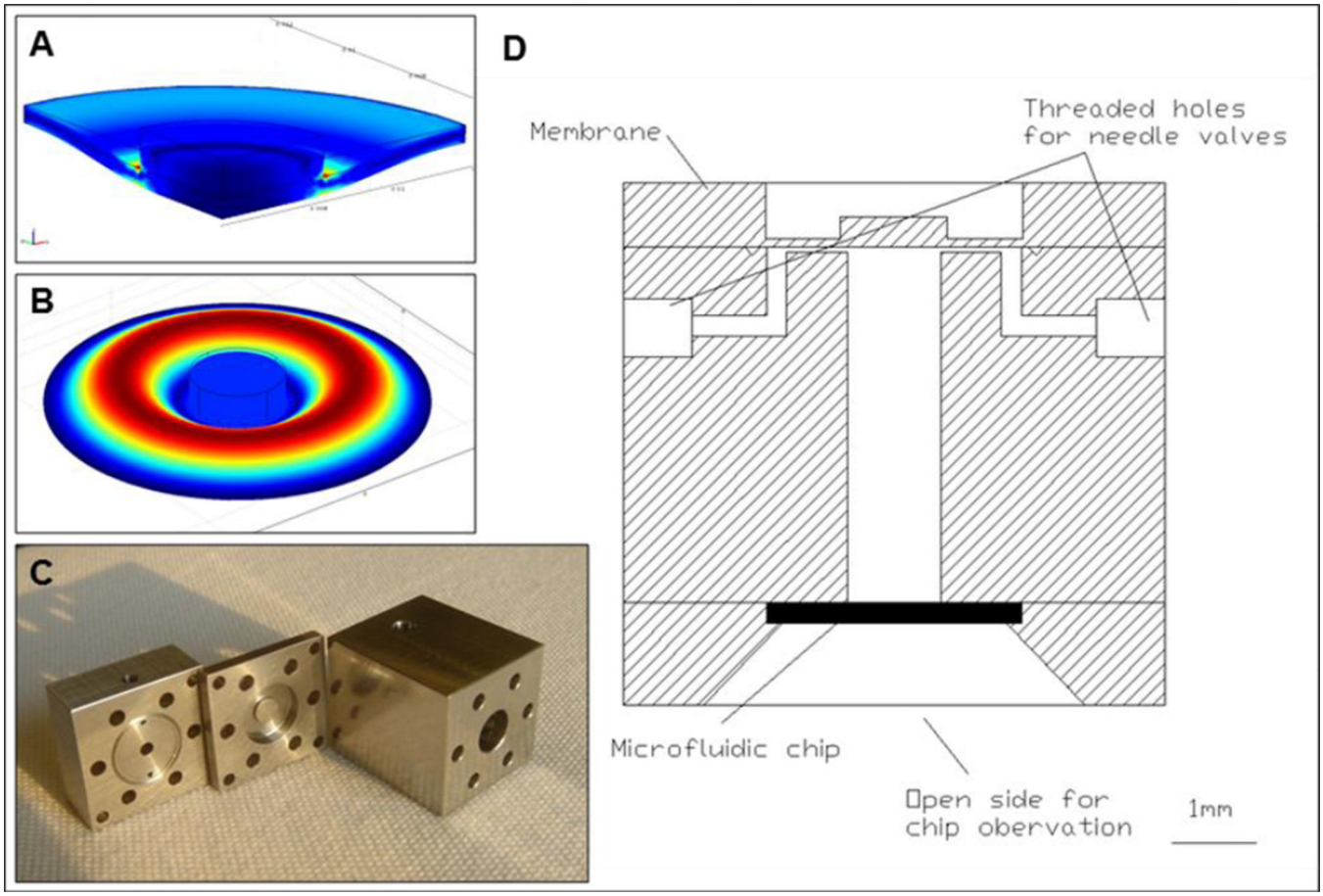

Figure 4.

Pressure chamber design. A)–B) Von Mises stress distribution into the loaded metal membrane. Deflection of the membrane compresses the fluid inside the chamber creating a jet through the outlet nozzle. Simulations were performed to make sure that stresses in the metal were below fatigue limits and to verify that buckling of the membrane would not occur as exemplified in B. C) Detail of the pressure chamber. From left, fluid reservoir, membrane, part for housing the piezo. D) Schematic cross section of the chip holder, pressure chamber and membrane.

NIH-PA Author Manuscript
NIH-PA Author Manuscript
NIH-PA Author Manuscript

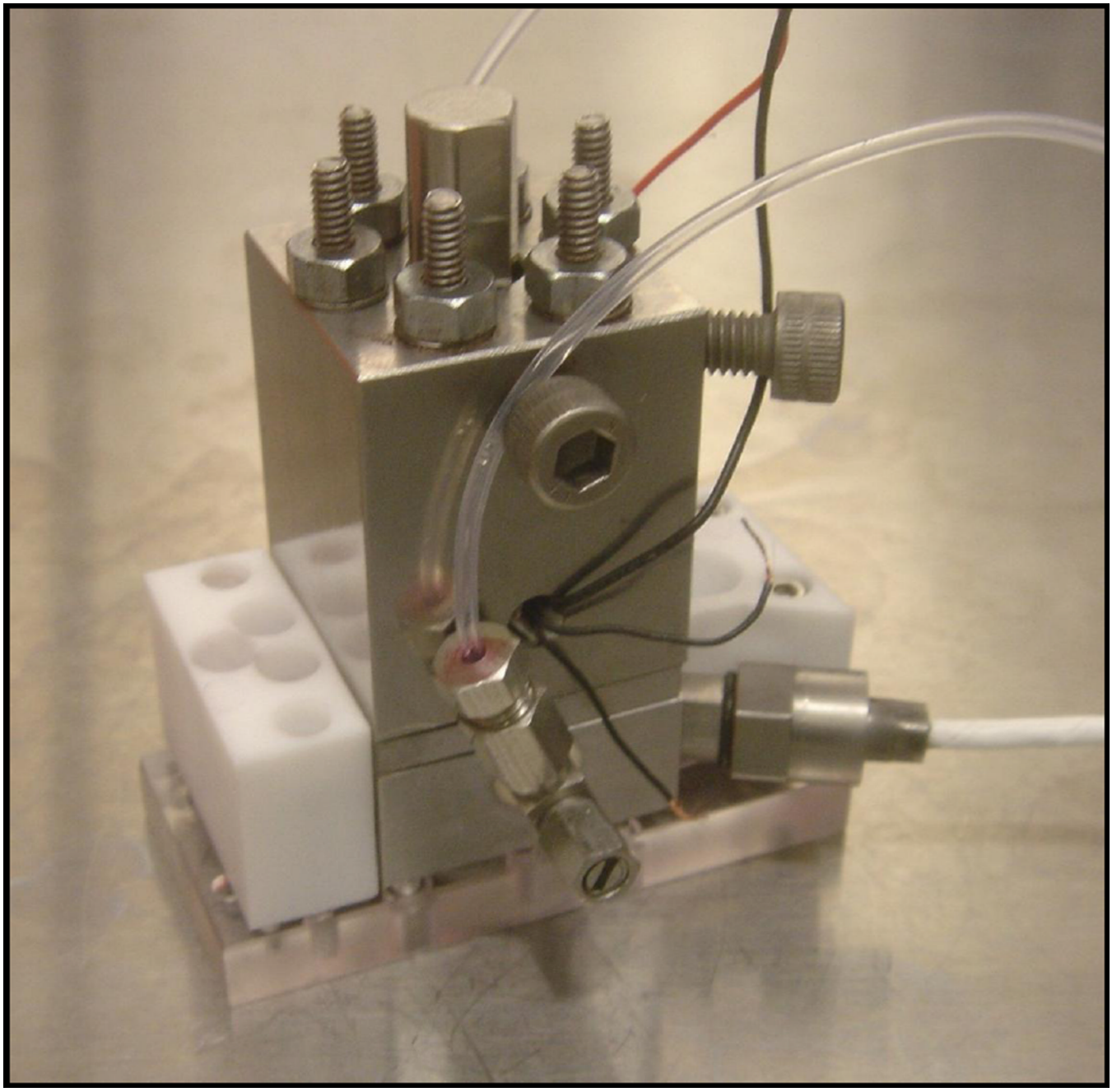

Figure 5.
Complete assembly of the pressure chamber with microfluidic chip holder and pressure sensor (with a white wire).

NIH-PA Author Manuscript

NIH-PA Author Manuscript

NIH-PA Author Manuscript

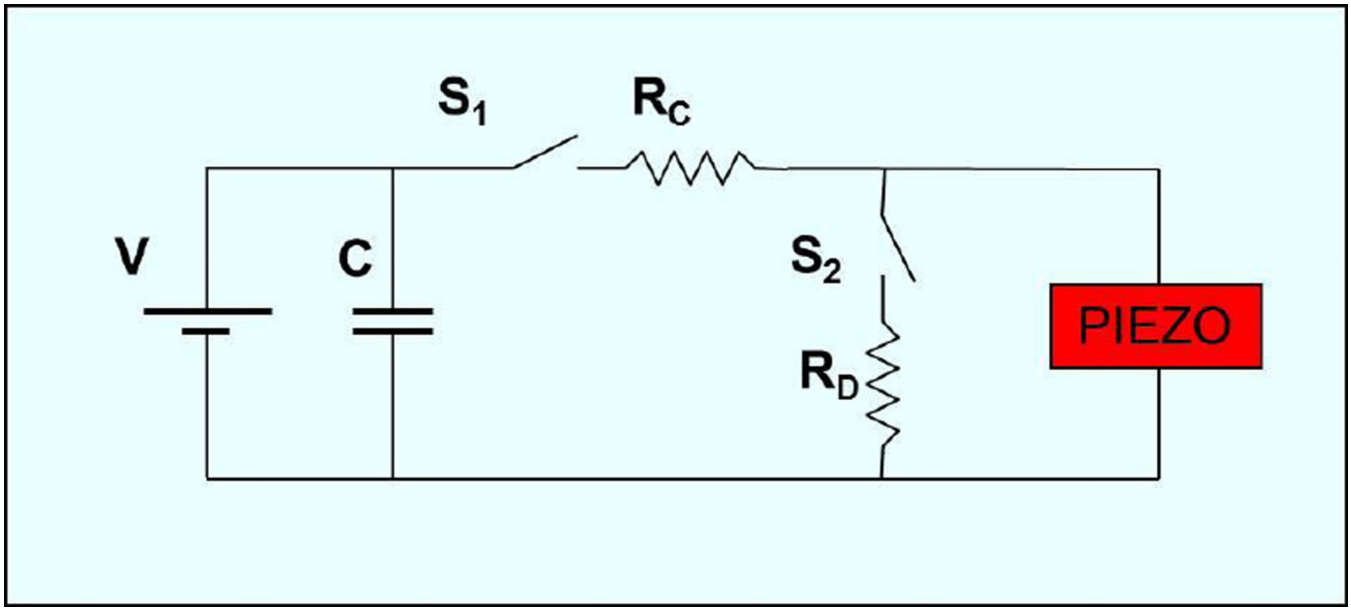

Figure 6.

Schematic of the circuit used to drive the piezoelectric actuator. V represents the power supply used to power the system and set the voltage. The power supply charges a large capacitor C that provides the instantaneous power required for actuation. S1 and S2 are synchronized switches. R_c and R_d are the resistances used to control time constants of charging and discharging respectively. Normally S1 is open and S2 is closed and therefore the piezo is at rest, upon actuation S2 is opened and S1 closed to allow charging of the piezo.

NIH-PA Author Manuscript
NIH-PA Author Manuscript
NIH-PA Author Manuscript

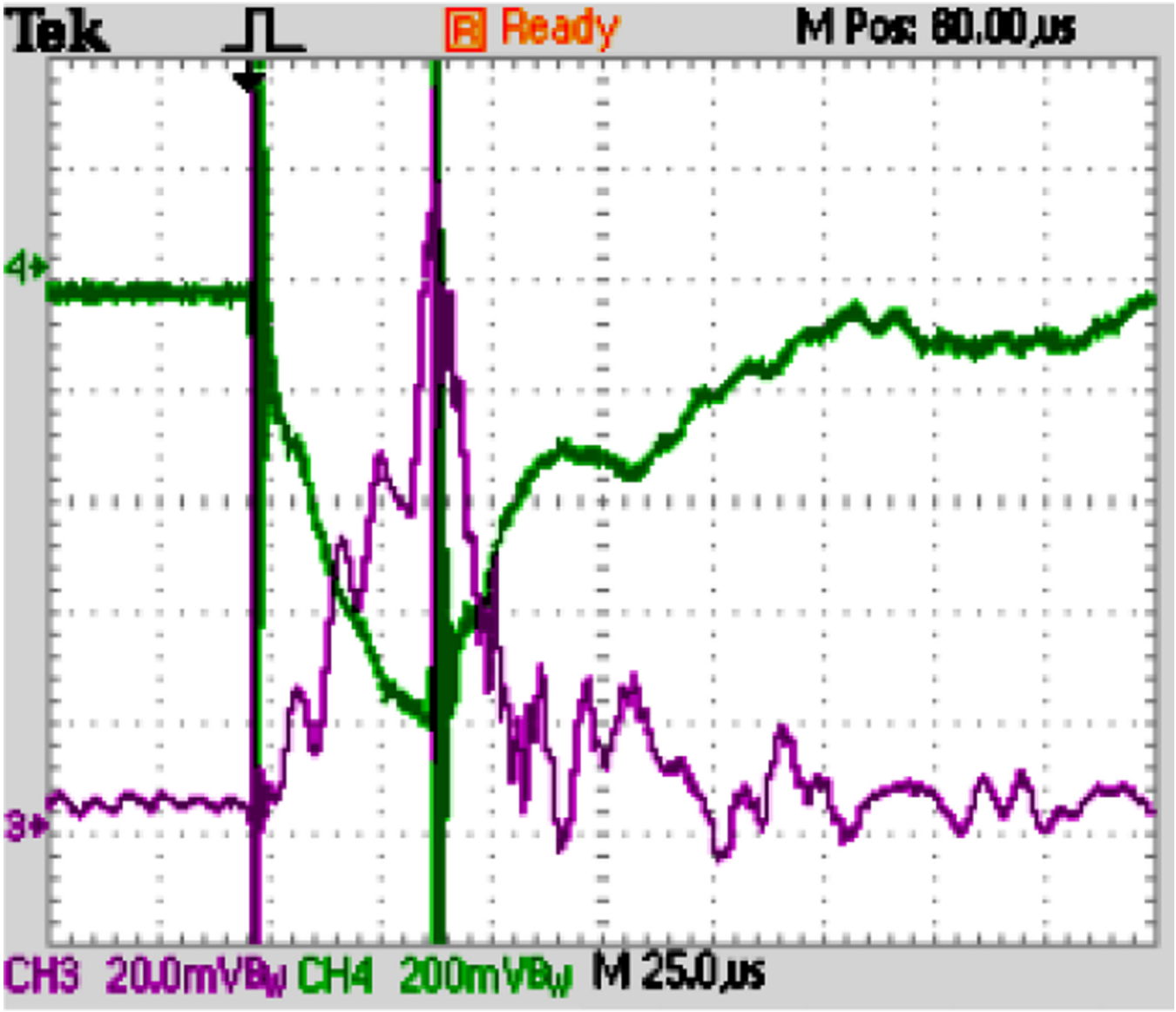

Figure 7.

Typical recording of the pressure in the chamber (purple) and piezo deformation (green) demonstrating that the system is able to generate pressure pulses up to ~35 bar in about 40 µs. Recordings were conducted in each experiment to monitor the behavior of the chamber. The strain gauge recordings of the piezo deformation closely corresponded to the pressure measurement and were mainly used to verify the activity of the piezo.

NIH-PA Author Manuscript

NIH-PA Author Manuscript

NIH-PA Author Manuscript

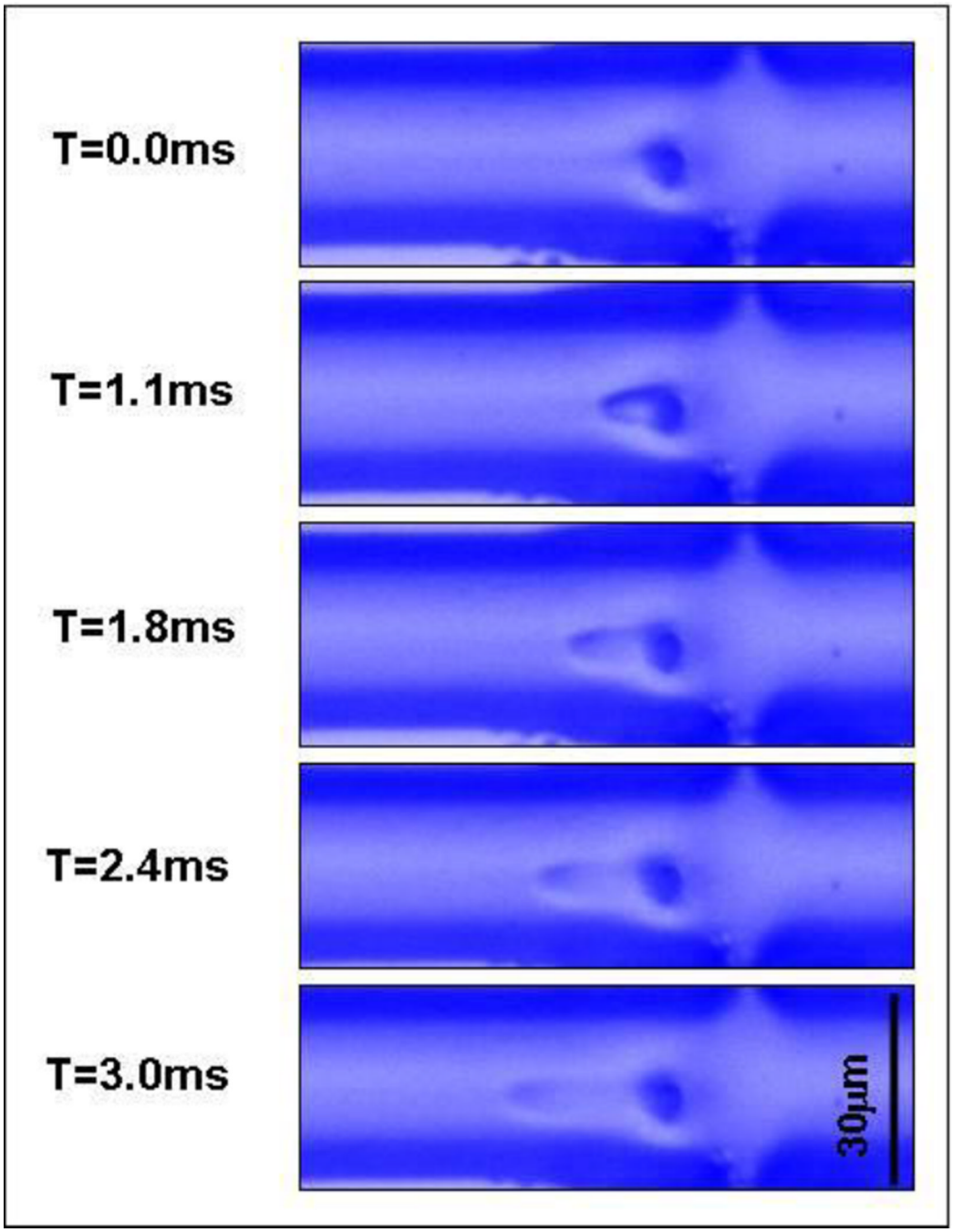

Figure 8.
Jet visualization experiments. Pure water is injected into a concentrated sucrose stream, the two solutions are miscible, but have a different refractive index allowing visualization of a droplet of pure water ejected into a stream of sucrose solution. Each frame corresponds to a different time after firing the jet. The droplet of water are ejected through the nozzle (dark point in each frame) in direction orthogonal to the paper and transported from right to left as a flow in that direction is established within the main channel.

NIH-PA Author Manuscript
NIH-PA Author Manuscript
NIH-PA Author Manuscript

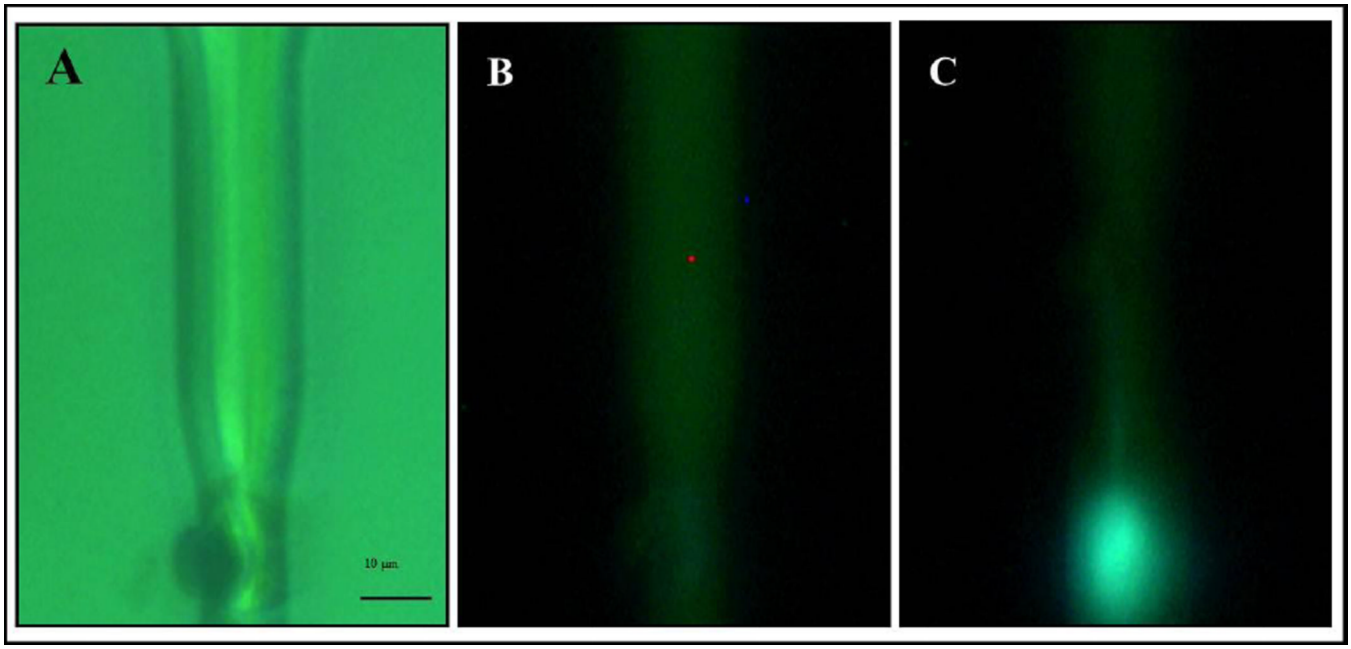

Figure 9.
Test of intracellular delivery. The ability of a jet to pierce a cell was tested firing a solution with a potassium indicator into a cell suspended in a potassium free buffer. A) Bright field picture of channel and cell. The cell is partially squeezed in a narrowing of the channel and is positioned in front of the micro nozzle B) Fluorescence picture just before firing a jet. C) Fluorescence image just after firing the jet. The indicator starts fluorescing after reacting with potassium present inside the cell. The fluorescence appears confined within the cell boundaries showing that the cell maintains its structure.

NIH-PA Author Manuscript
NIH-PA Author Manuscript
NIH-PA Author Manuscript

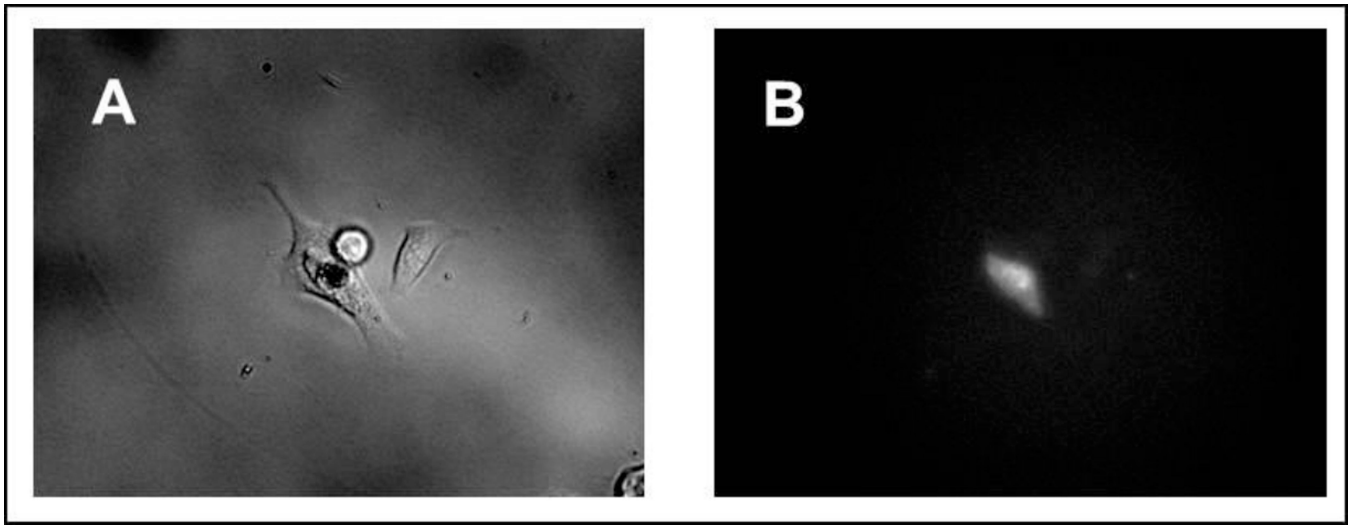

Figure 10.
Injection results. A) bright field image of HeLa cell "jet-injected" with fluorescent dextran conjugate 24h after treatment, and B) fluorescence image of the same cultured cell. Notice that the cell has reattached to the culture plate.